Science Advances
AAAS

advances.sciencemag.org/cgi/content/full/5/9/eaax2742/DC1

Supplementary Materials for

High-performance suction feeding in an early elasmobranch

Michael I. Coates*, Kristen Tietjen, Aaron M. Olsen, John A. Finarelli

*Corresponding author. Email: mcoates@uchicago.edu

Published 11 September 2019, *Sci. Adv.* **5**, eaax2742 (2019)
DOI: 10.1126/sciadv.aax2742

The PDF file includes:

Other Supplementary Material for this manuscript includes the following:

(available at advances.sciencemag.org/cgi/content/full/5/9/eaax2742/DC1)

SUPPLEMENTARY FIGURES

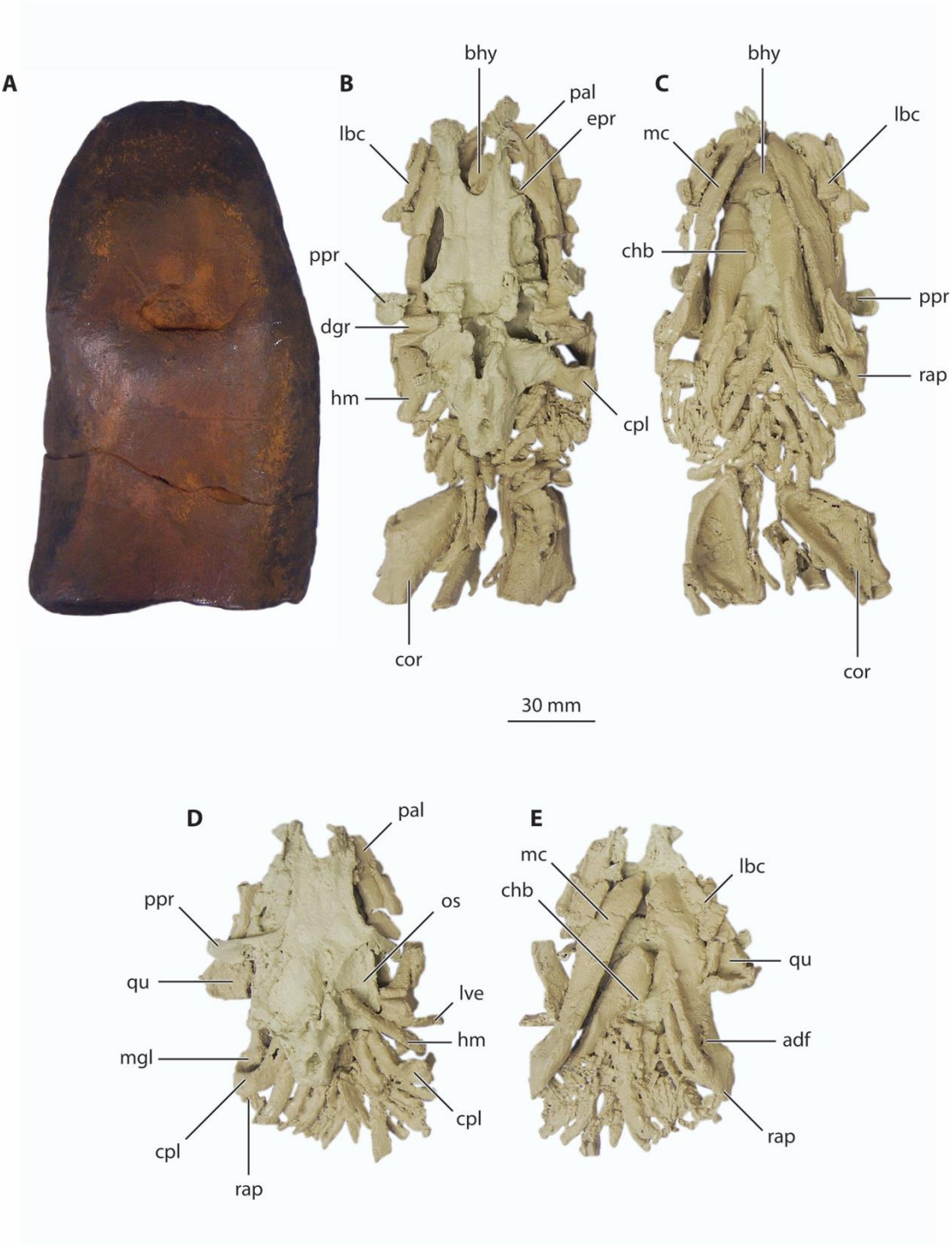

Fig. S1. *Tristychius arcuatus*, renderings of key specimens. (**A**) Complete concretion (NMS 1974.23.6). (**B**) Rendered pectoral, branchial and cranial cartilages in dorsal view (NMS 1974.23.6) and (**C**) ventral view. (**D**) Rendered branchial and cranial cartilages in dorsal view (NMS 1974.23.20) and (**E**) ventral view. adf, adductor fossa; bhy, basihyal; chb, ceratohyal blade; cor, coracoid; cpl, ceratohyal platform; dgr, dorsal groove; epr, ethmoid process; hm, hyomandibula; lbc, labial cartilage chain; lve, lateroventral extremity of palatoquadrate; mc, Meckel's cartilage; mgl, mandibular glenoid; os, otic shelf; pal, palatine process; ppr, postorbital process; qu, quadrate; rap, retroarticular process.

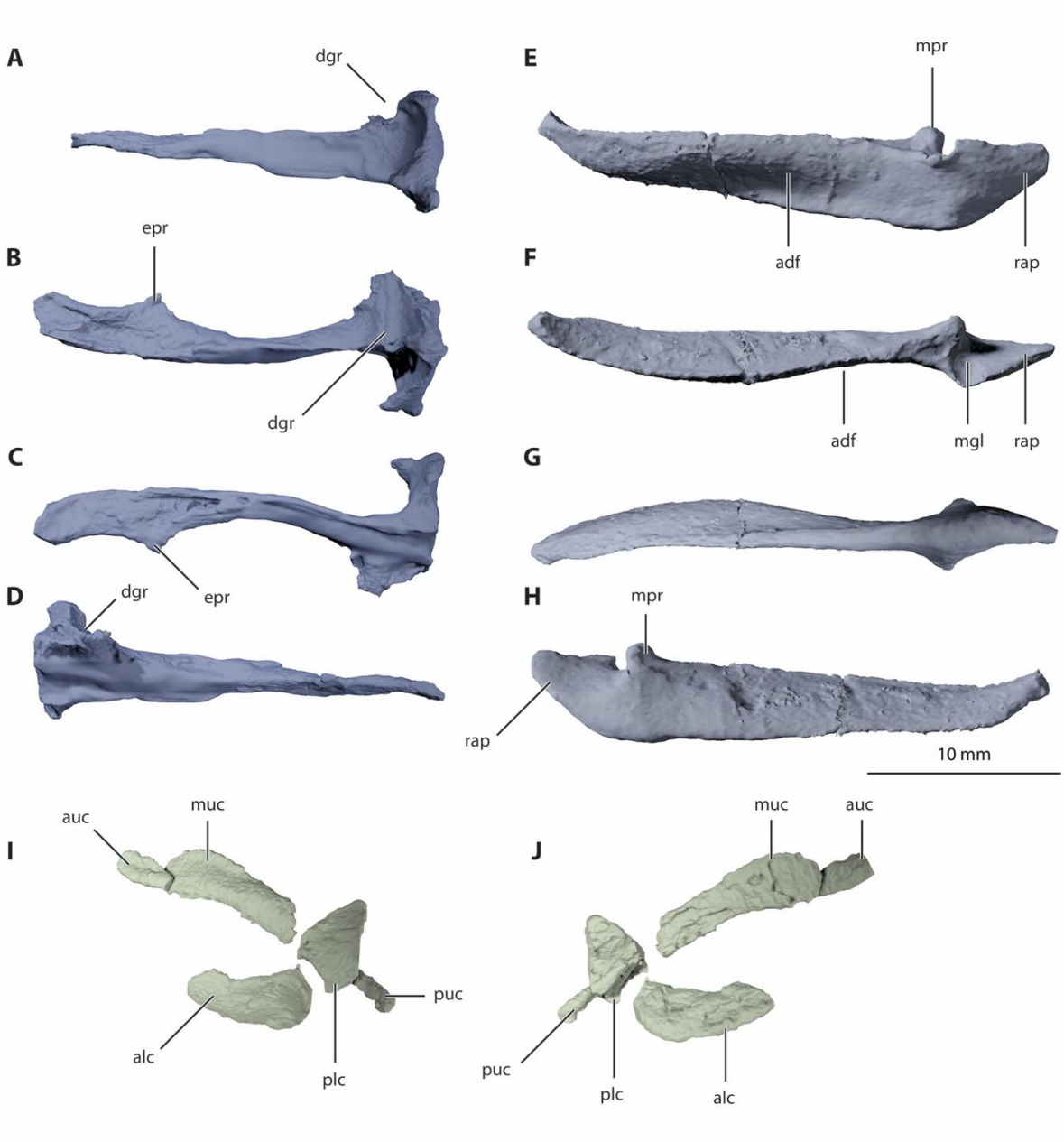
A
dgr
B
epr
dgr
C
epr
D
dgr
E
mpr
adf
rap
F
adf
mgl
rap
G
H
mpr
rap
10 mm
I
auc
muc
puc
alc
plc
J
muc
auc
puc
plc
alc

Fig. S2. Mandibular arch cartilages of *T. arcuatus*. Left palatoquadrate (NMS 1974.23.6) in (**A**) lateral, (**B**) dorsal, (**C**) ventral, and (**D**) ventral views. Left Meckel's cartilage (NMS 1974.23.6) in (**E**) lateral, (**F**) dorsal, (**G**) ventral, and (**H**) mesial views. Left labial cartilage chain (NMS 1974.23.6) in (**I**) lateral and (**J**) mesial views. adf, adductor fossa; dgr, dorsal groove; epr, ethmoid process; mgl, mandibular glenoid; mpr, mandibular process; rap, retroarticular process. Labial cartilage chain: alc, anterior lower cartilage; auc, anterior upper cartilage; muc, middle upper cartilage; plc, posterior lower cartilage; puc, posterior upper cartilage.

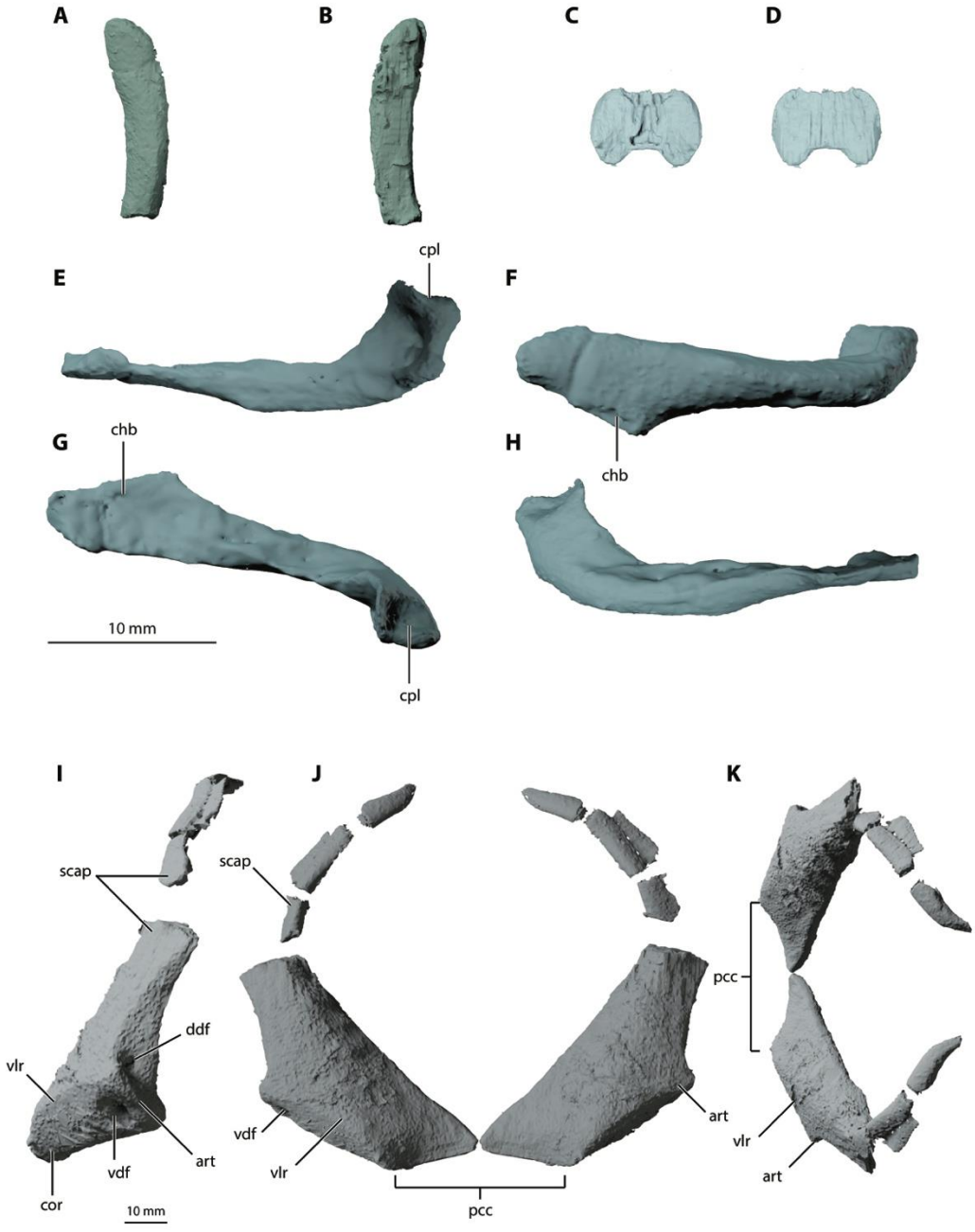
A
B
C
D
E
cpl
F
G
chb
H
chb
10 mm
cpl
I
J
K
scap
scap
pcc
ddf
vlr
vdf
art
cor
10 mm
vdf
vlr
art
pcc
vlr
art

Fig. S3. Hyoid arch and pectoral girdle of *T. arcuatus*. Left hyomandibula (NMS 1974.23.6) in (**A**) lateral and (**B**) mesial views. Basihyal in (**C**) dorsal and (**D**) ventral views (NMS 1974.23.6). Left ceratohyal (NMS 1974.23.30) in (**E**) lateral, (**F**) ventral, (**G**) dorsal and (**H**) mesial views. Pectoral girdle in (**I**) left side lateral, (**J**) anterior, and (**K**) dorsal views (NMS 1974.23.6). For pectoral girdle comparison and terminology see Lane *et al*. (*77*). art, articular condyle; chb, ceratohyal blade; cor, coracoid; cpl, ceratohyal platform (articular surface for distal end of hyomandibula); ddf, dorsal diazonal foramen; pcc, pericardial concavity; scap, scapular process; vdf, ventral diazonal foramen; vlr, ventrolateral ridge.

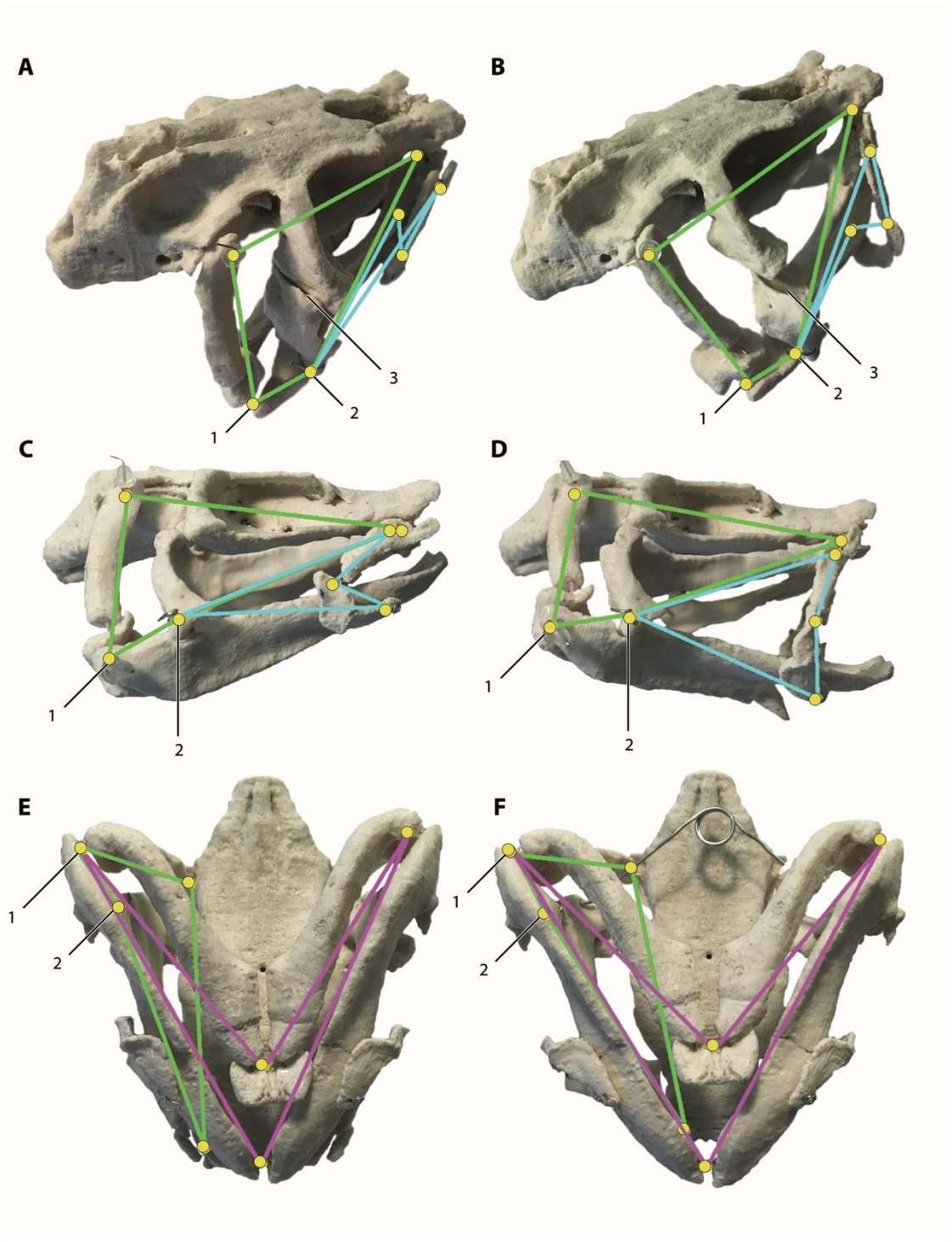
A
1
2
3
B
1
2
3
C
1
2
D
1
2
E
1
2
F
1
2

Fig. S4. *T. arcuatus*: physical model showing interconnected 3D four-bar linkages. Posterodorsal and lateral view, (**A**) jaws closed and (**B**) open. Lateral view, (**C**) jaws closed and (**D**) open. Ventral view, (**E**) jaws closed and (**F**) open. Coloured bars delineate interconnected four-bar linkage systems. Green bars: hyomandibula-neurocranium-palate-mandible. Cyan bars: palate-upper labials -lower labials-mandible. Pink bars: right mandible-right ceratohyal-left ceratohyal-left mandible. Green and cyan linkage systems interconnect through the mandibulo-hyoid joint (1). Green and blue linkage systems interconnect through the jaw joint (2). Ridge and groove sliding articulation (3).

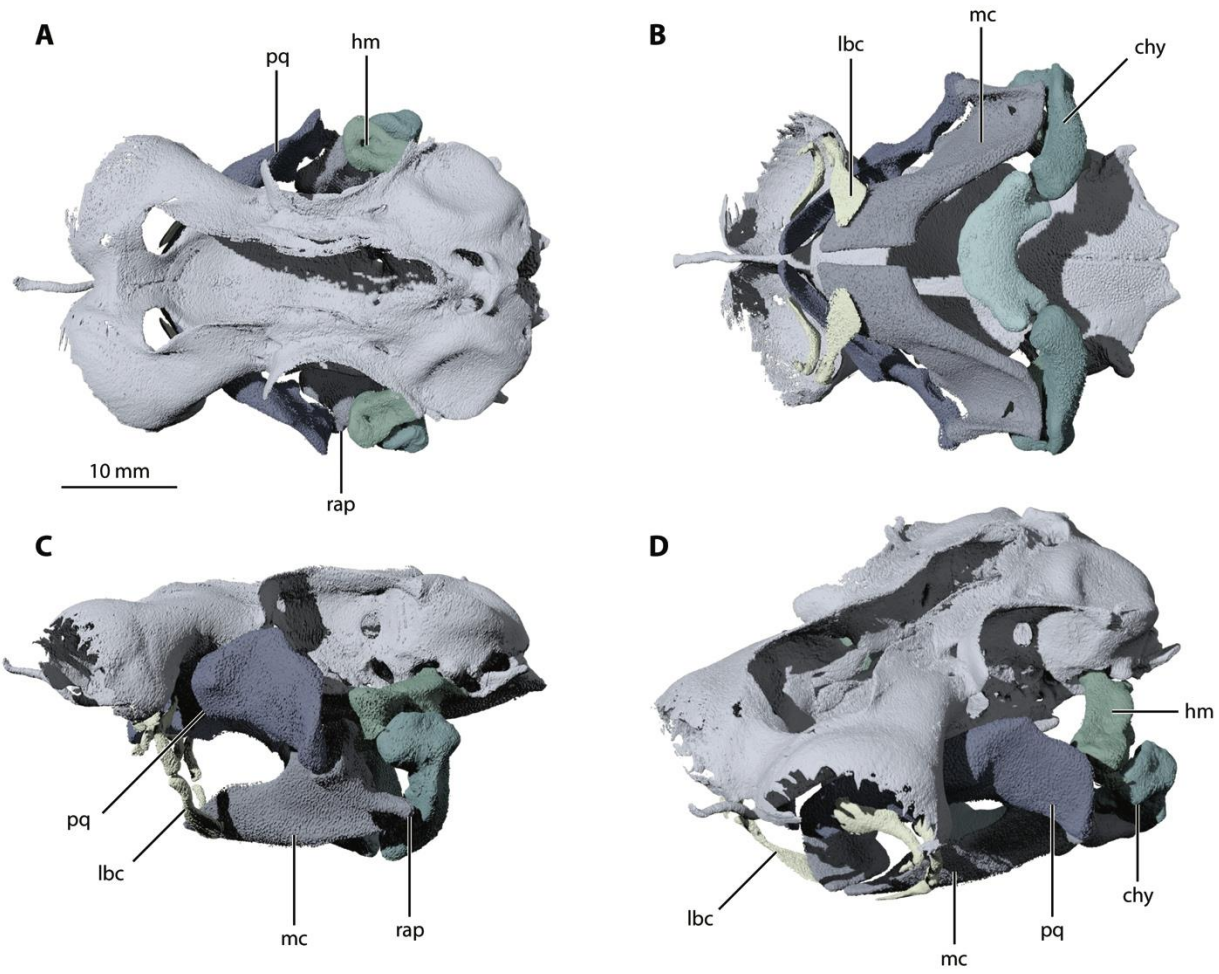

Fig. S5. The cranial skeleton of a juvenile *Chiloscyllium punctatum* reconstructed from high-resolution computed tomography. (**A**) Dorsal view; (**B**) ventral view; (**C**) left lateral view; (**D**) anterior dorsolateral view. chy, ceratohyal; hm, hyomandibula; lbc, labial cartilage chain; mc, Meckel's cartilage; pq, palatoquadrate; rap, retroarticular process.

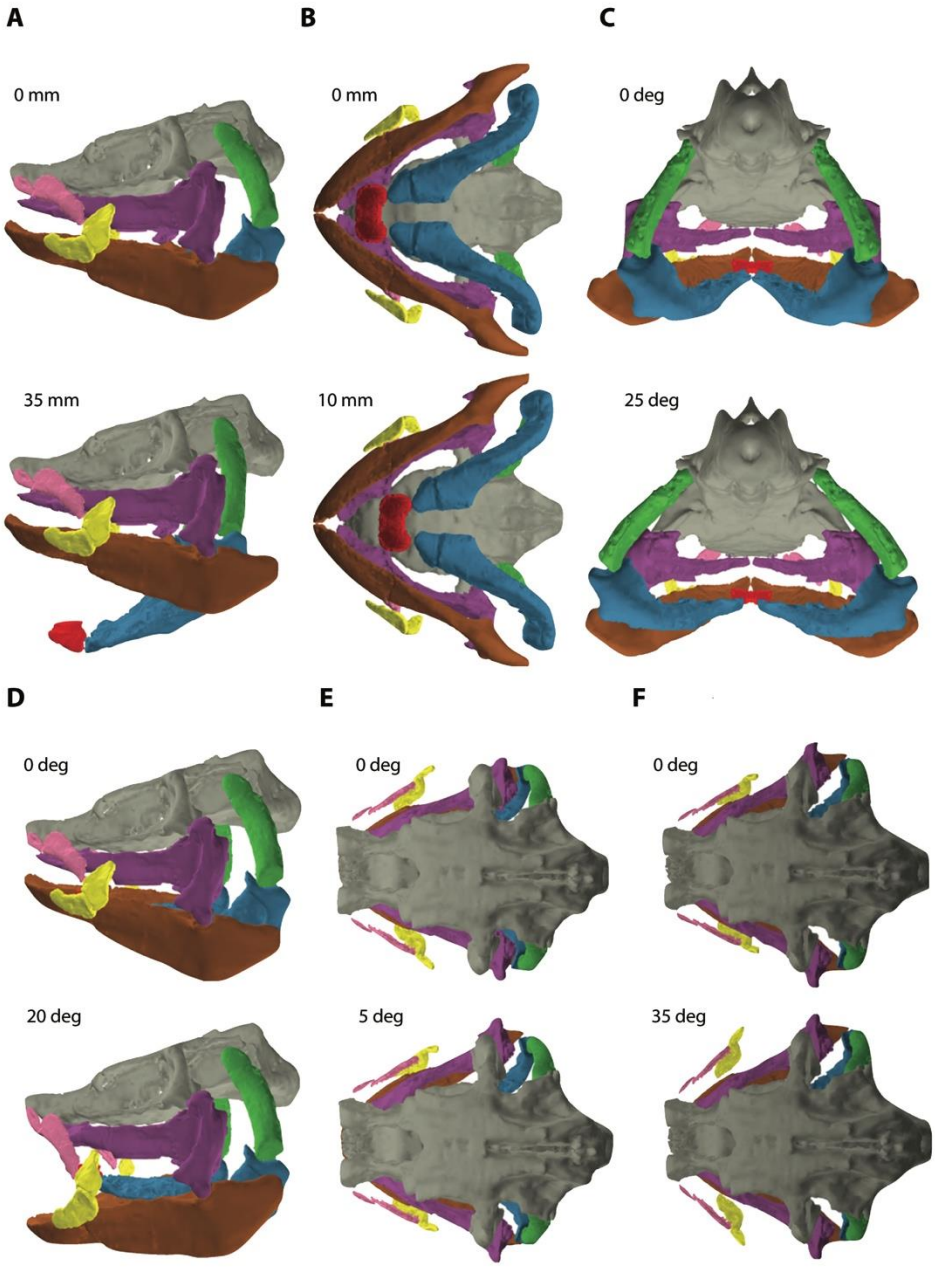
A
B
C
0 mm
0 mm
0 deg
35 mm
10 mm
25 deg
D
E
F
0 deg
0 deg
0 deg
20 deg
5 deg
35 deg

Fig. S6. Conformations of the skull of *T. arcuatus*. The cranial cartilages of *T. arcuatus* likely had at least 6 primary degrees of freedom of motion. (**A**) basihyal ventral translation; (**B**) basihyal caudal translation; (**C**) hyoid arch abduction; (**D**) Meckel's cartilage depression; (**E**) mandibular arch abduction; (**F**) labial cartilage flaring. Each of these motions is shown, independently, at the limits of their simulated range of movement.

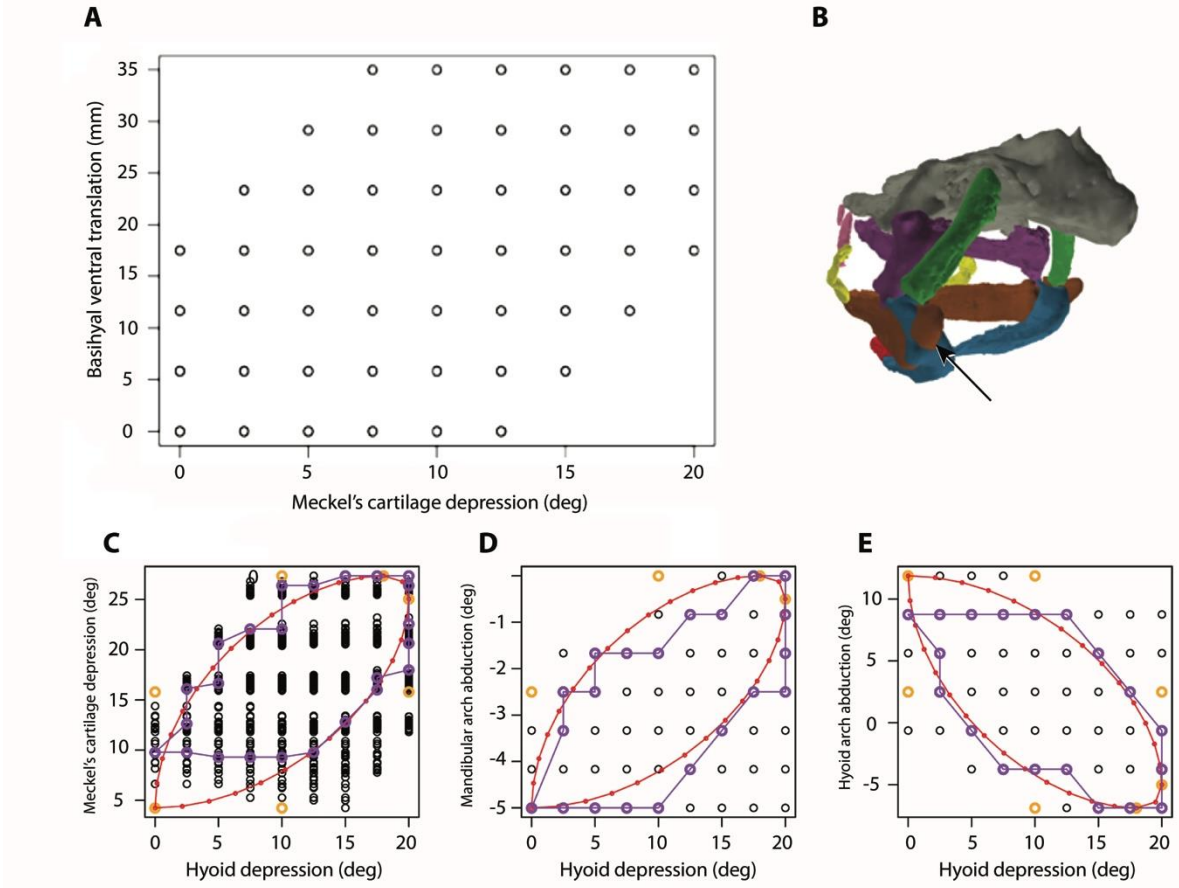
A
Basihyal ventral translation (mm)
Meckel's cartilage depression (deg)
B
C
Meckel's cartilage depression (deg)
Hyoid depression (deg)
D
Mandibular arch abduction (deg)
Hyoid depression (deg)
E
Hyoid arch abduction (deg)
Hyoid depression (deg)

Fig. S7. Filtering the dataset of *T. arcuatus* cranial conformations. (**A**) The first criterion used to filter the multidimensional skull conformation set: each point represents a set of conformations at that particular combination of the Meckel's depression and basihyal ventral translation. Open triangular spaces in the top left and bottom right indicate conformations that were removed from the full conformation set. (**B**) Example of interpenetrating meshes; arrow shows intersection of ceratohyal and Meckel's cartilage. Conformations with interpenetration were filtered out of the skull conformation set. (**C**, **D**, and **E**) Paths or trajectories traced through a 5-dimensional skull conformation space to create a motion sequence. Red line and points: the motion path as a Bézier spline; orange points: Bézier spline control points; purple line and points: closest points in conformation space to the path.

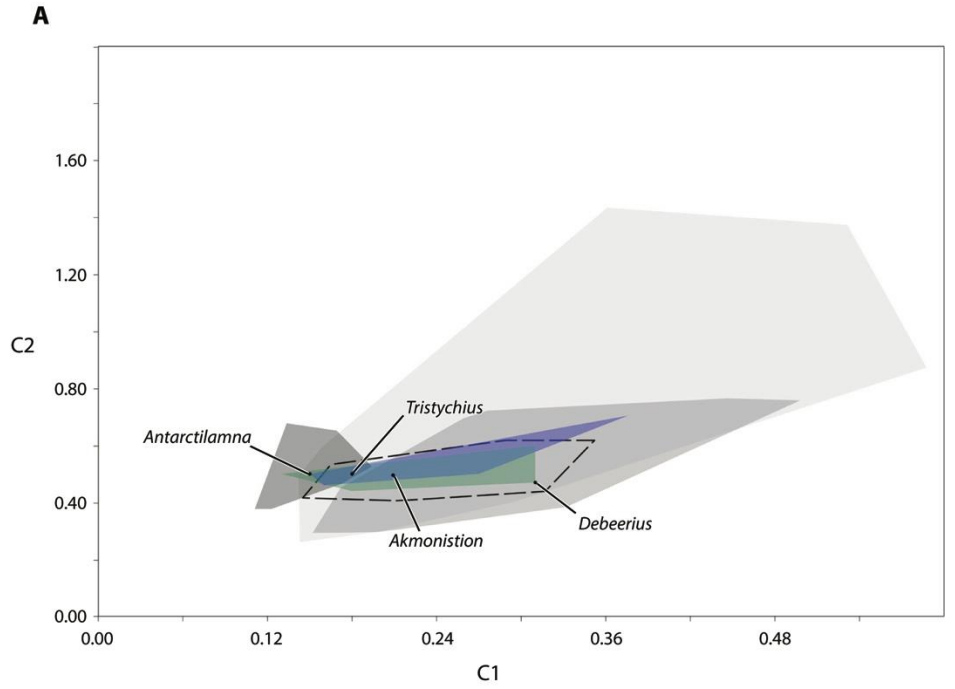
A
1.60
1.20
C2
0.80
0.40
0.00
0.00
0.12
0.24
0.36
0.48
C1
Tristychius
Antarctilamna
Debeerius
Akmonistion

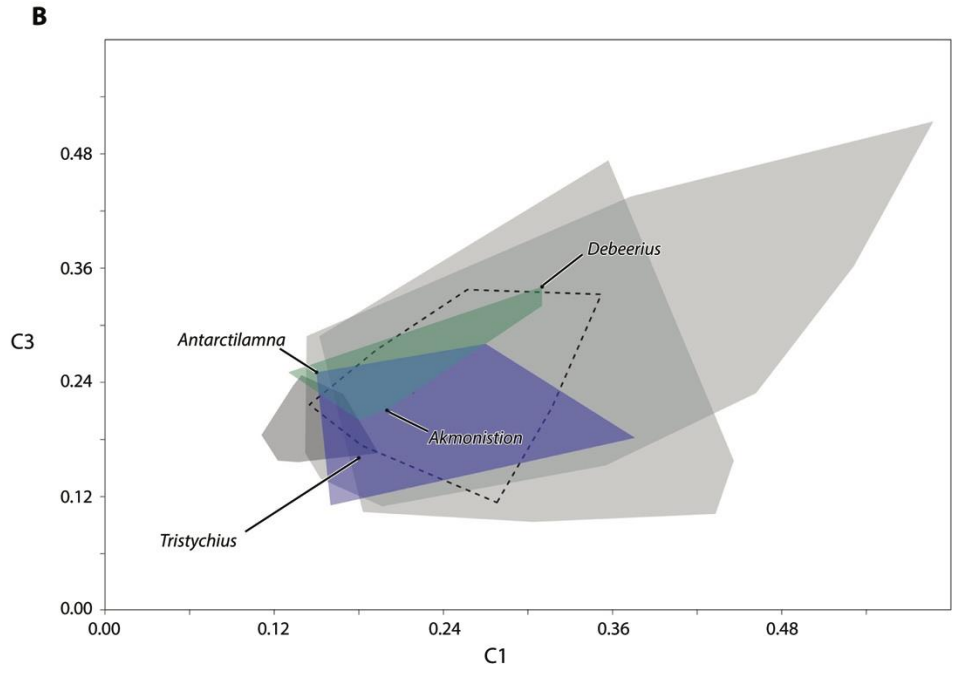
B
0.48
0.36
C3
0.24
0.12
0.00
0.00
0.12
0.24
0.36
0.48
C1
Debeerius
Antarctilamna
Akmonistion
Tristychius

Fig. S8. Morphospace for early gnathostomes relative to jaw measurement characters from Anderson *et al.* (*36*). (**A**) Measurements C1 vs. C2. (**B**) Measurements C1 vs. C3. Data supplement in table S3. Gray regions, from lightest to darkest, are sarcopterygians, placoderms and actinopterygians. The remaining polygons represent the greater chondrichthyan radiation (*16*, *60*): acanthodians in the dashed region, holocephalans in green, and elasmobranchs in blue, with several early chondrichthyan taxa highlighted. Note that *Tristychius*, when plotted in this morphospace does not stand out as particularly different from the rest of the elasmobranch taxa, despite presenting a jaw morphology not observed in any other elasmobranch in this data set. This serves to highlight the shortcomings of 2D morphometric data (in this case, chords measured in lateral view) to describe the complex 3D morphologies (*38*, *40*).

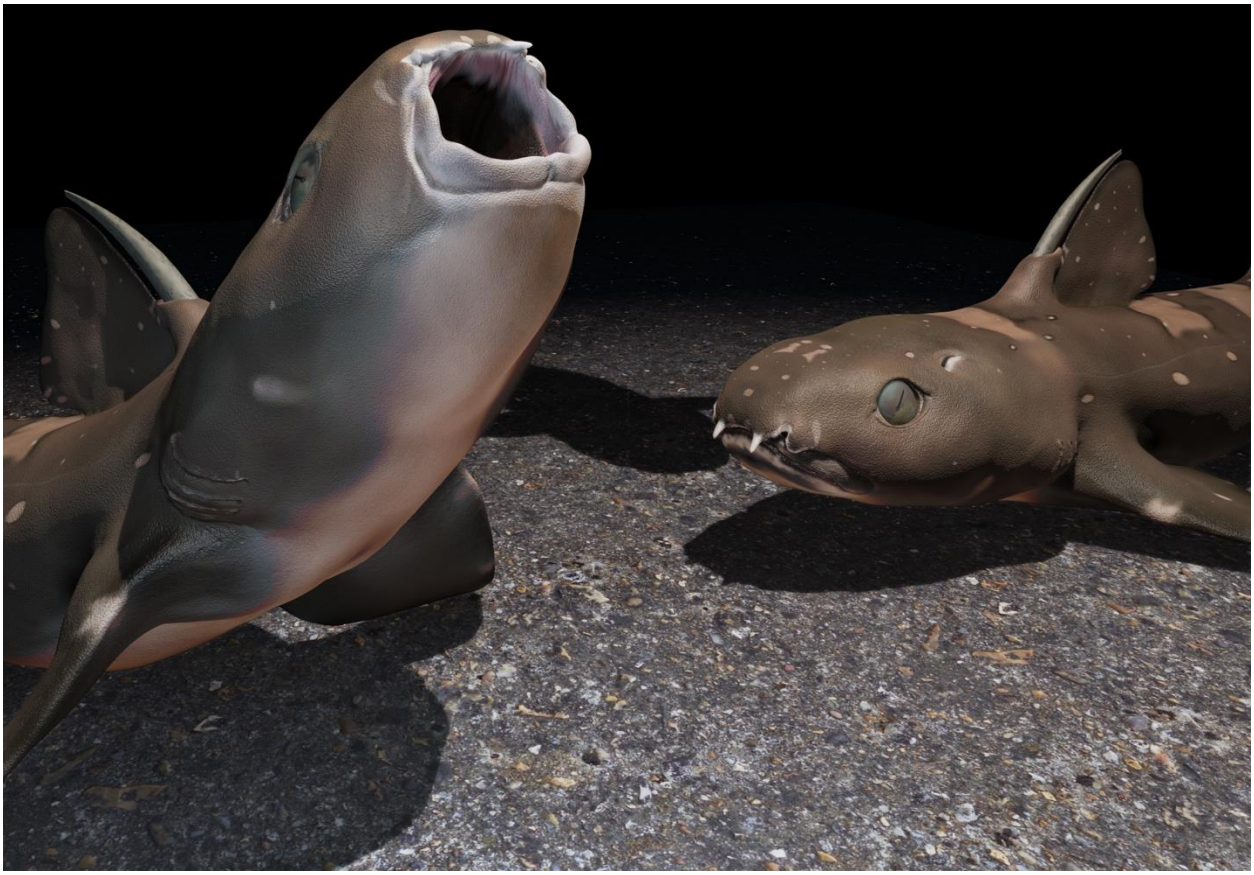

Fig. S9. Life restoration of *T. arcuatus* from the Viséan Wardie Shales of Edinburgh, Scotland.

SUPPLEMENTARY TABLES

Table S1. *T. arcuatus* specimens contributing to study.

National Museum of Scotland catalogue number	Field number	Figured	Summary notes
1972.27.461A, B	SPW 171a, b	Dick (*12*), Text-Fig. 11.	Cranium to pectoral girdle; external surfaces of cartilage, but contents absent. Scans poor.
1972.27.481A-E		Dick (*12*), Text-Fig. 8A. Coates & Tietjen (*13*), Figs 2, 7a, 8, 9, 11a-d.	Neurocranium; jaws and hyoid arch; hyoid rays and gill arch rays; exceptionally complete gill skeleton; pectoral parts. Lateral compression. Scans good.
1974.23.6		Coates & Tietjen (*13*), Fig. 5.	Neurocranium; jaws and hyoid arch; hyoid rays and gill arch rays; complete gill skeleton; pectoral parts. Dorsoventral compression. Scans good.
1974.23.30A, B	SPW 730	Coates & Tietjen (*13*), Fig. 6a-c.	Neurocranium; jaws and hyoid arch; hyoid rays and gill arch rays; complete gill skeleton. Dorsoventral compression. Scans good.

1974.51.2A, B	SPW 863a, b	Coates & Tietjen (*13*), Fig. 6d-f.	Neurocranium. Dorsoventral compression. Scans good.
G2015.30.1		Coates & Tietjen (*13*), Fig. 4, 7b, 10.	Neurocranium. Dorsoventral compression. Scans good.

Table S2. Measurements of oral volume (milliliters) from physical model of *T. arcuatus*. 10 trials; final column = average score; Meckel's cartilage length: 100mm.

Mouth closed	105	100	98	92	97	96	101	99	104	90	98.2
Meckel's cartilage 22^{o} Ceratohyal 25^{o}	150	146	140	142	153	137	147	154	150	146	146.5
Meckel's cartilage 18^{o} Ceratohyal 32^{o}	155	157	167	154	160	153	166	161	169	161	160.3
Meckel's cartilage 6^{o} Ceratohyal 19^{o}	133	131	135	119	126	128	134	120	123	119	126.8
Labial cartilage and cheek enclosure	32										

Table S3. Additions to Anderson *et al.* (*36*) dataset of mandible metrics.

Taxon	Source	Age	C1	C2	C3
Akmonistion	Coates & Sequeira (*61*).	Serpukhovian	0.2	0.5	0.21
Antarctilamna	Young (*68*).	Givetian	0.15	0.5	0.25
Cobelodus	Zangerl & Case (*69*).	Moscovian	0.16	0.5	0.17
Damocles	Lund (*70*).	Serpukhovian	0.13	0.5	0.25
Debeerius	Grogan & Lund (*9*).	Serpukhovian	0.31	0.47	0.34
Diplodoselache	Dick (*55*).	Viséan	0.2	0.5	0.23
Falcatus	Lund (*71*).	Serpukhovian	0.18	0.44	0.20
Gladbachus	Coates et al. (*16*).	Givetian	0.21	0.5	0.16
Gogoselachus	Long et al. (*72*).	Frasnian	0.2	0.49	0.23
Helicoprion	Tapinala et al. (*73*).	Guadalupian	0.27	0.5	0.28
Orthacanthus	Hotton (*62*).	Kasimovian	0.21	0.5	0.25
Sibyrhynchid	Pradel (*74*).	Gzhelian	0.31	0.6	0.32
Thrinacoselache	Grogan & Lund (*75*).	Serpukhovian	0.16	0.46	0.11
Triodus	Heidtke et al.	Kasimovian	0.21	0.5	0.23

	(*76*).				
Tristychius	Dick (*12*) and current	Viséan	0.18	0.5	0.16

SUPPLEMENTARY MOVIES

Movie S1. Jaw and hyoid motion sequences modeled in caudal view. Movement constraints at cranial joints described in Materials and Methods section: Virtual simulation methods.

Movie S2. Jaw and hyoid motion sequences modeled in cranial view. Movement constraints at cranial joints described in Materials and Methods section: Virtual simulation methods.

Movie S3. Jaw and hyoid motion sequences modeled in dorsal view. Movement constraints at cranial joints described in Materials and Methods section: Virtual simulation methods.

Movie S4. Jaw and hyoid motion sequences modeled in lateral view. Movement constraints at cranial joints described in Materials and Methods section: Virtual simulation methods.

Movie S5. Jaw and hyoid motion sequences modeled in ventral view. Movement constraints at cranial joints described in Materials and Methods section: Virtual simulation methods.

Movie S6. Animation of complete cranial to pectoral skeleton opening and closing jaws, ingesting prey. Sequence of movements follows motion sequence described in Fig. 3; timing, with rapid expansive and slower compressive phases, after observations by Motta *et al*. (*29*); pectoral shrug after Camp *et al.* (*24*).